Coronary Motion Estimation from CTA Using Probability Atlas and Diffeomorphic Registration

Dong Ping Zhang[1], Laurent Risser[1,2], François-Xavier Vialard[2]
Philip Edwards[1], Coert Metz[3], Lisan Neefjes[4]
Nico Mollet[4], Wiro Niessen[3], and Daniel Rueckert[1]

[1] Department of Computing, Imperial College London, London, UK
[2] Institute for Mathematical Science, Imperial College London, London, UK
[3] Dept. of Medical Informatics and Radiology, Erasmus MC, Rotterdam, NL
[4] Dept. of Radiology and Cardiology, Erasmus MC, Rotterdam, NL

Abstract. In this paper, we present a method for coronary artery motion estimation from 4D cardiac CT angiogram (CTA) data sets. The proposed method potentially allows the construction of patient-specific 4D coronary motion model from pre-operative CTA which can be used for guiding totally endoscopic coronary artery bypass surgery (TECAB). The proposed approach consists of three steps: Firstly, prior to motion tracking, we form a coronary probability atlas from manual segmentations of the CTA scans of a number of subjects. Secondly, the vesselness response image is calculated and enhanced for end-diastolic and end-systolic CTA images in each 4D sequence. Thirdly, we design a special purpose registration framework for tracking the highly localized coronary motion. It combines the coronary probability atlas, the intensity information from the CTA image and the corresponding vesselness response image to fully automate the coronary motion tracking procedure and improve its accuracy. We performed pairwise 3D registration of cardiac time frames by using a multi-channel implementation of the Large Deformation Diffeomorphic Metric Mapping (LDDMM) framework, where each channel contains a given level of description of the registered shapes. For validation, we compare the automatically tracked coronaries with those segmented manually at end-diastolic phase for each subject.

1 Introduction

As one of the leading causes of death worldwide, coronary artery disease occurs due to the failure of the blood circulation to supply adequate oxygen and nutrition to cardiac tissues. It is typically caused by the excessive accumulation of atheromatous plaques and fatty deposits within certain regions of the arteries which restrict the blood flow. To treat this disease, arteries or veins grafted from the patient's body are used to bypass the blockages and restore the supply to the heart muscle. Conventional bypass surgery requires invasive sternotomy and the use of a cardiopulmonary bypass machine, which leads to

H. Liao et al. (Eds.): MIAR 2010, LNCS 6326, pp. 78–87, 2010.

long recovery period for the patient and has high infectious potential. Using image-guided robotic surgical system, totally endoscopic coronary artery bypass (TECAB) surgery techniques have been developed to allow clinicians to perform bypass surgery off-pump with three pin-hole incisions in the chest cavity, through which two robotic arms and one stereo endoscopic camera are inserted. However, 20-30% conversion rates from TECAB surgery to conventional invasive surgical approach [1,2] have been reported due to the vessel misidentification and mislocalization caused by the restricted field of view of the stereo endoscopic images. To reduce this conversion rate and facilitate the TECAB procedure, we aim to construct a patient-specific 4D coronary artery motion model from preoperative cardiac CTA sequence. The main challenge of constructing this motion model is to follow the motion and deformation of the coronaries from end-systolic to end-diastolic phase accurately. In this paper, we propose a pyramid registration framework to achieve this. Finally, through temporally and spatially aligning the coronary motion model with the intraoperative endoscopic views of the patient's beating heart, this work has the potential to assist the surgeon to identify and locate the correct coronaries during the robotically-controlled TECAB procedures.

1.1 Related Work

Recent advances in computed tomography of coronary arteries [3] have attracted several studies on using CTA for coronary artery disease diagnosis and surgical planning. Extensive reviews on coronary artery segmentation are given in Schaap *et al.* [4] and Lesage *et al.* [5]. Although coronary artery segmentation has been well studied, particularly in the Grand Challenge of Coronary Artery Centerline Extraction [6], constructing motion models of coronaries from pre-operative CTA sequences to assist the diagnosis and surgery is a topic which has received less attention. The work in this paper differs significantly from 3D vessel segmentation approaches: our aim is not the extraction of the coronaries in single-phase high-quality CTA datasets as in [6], but instead estimating the coronary motion from end-systolic to end-diastolic phase in multi-phase cardiac CTA sequence.

Previously, Shechter *et al.* [7,8] tracked coronary artery motion in a temporal sequence of biplane X-ray angiography images. In their approach, a 3D coronary model is reconstructed from extracted 2D centrelines in end-diastolic angiography images. The deformation throughout the cardiac cycle is then recovered by a registration-based motion tracking algorithm. The limitation of this approach is that 3D reconstruction of the coronary from 2D X-ray images is required. An alternative approach for the extraction of the coronaries from cardiac CTA has been proposed by Metz *et al.* [9]: Here the coronaries are manually or semi-automatically identified at one time frame and then tracked throughout the cardiac cycle using non-rigid registration of the multi-phase cardiac CTA images. The restriction of this approach is that highly localized motion of the coronaries cannot be fully recovered by the motion tracking of the entire heart, particularly for right coronary artery as shown in Fig. 2 and Fig. 3 in [9].

In this paper, we present a novel approach for automatic segmentation of the coronary lumen and motion tracking of the coronaries from end-systolic to end-

diastolic phase in 4D cardiac CTA images. This is achieved by using tensor voting to improve the connectivity of the coronary vessels in vesselness response image and a special-purpose registration framework for coronary motion tracking. The advantages of the proposed approach here are two folds. Firstly, it contains less manual pre-processing procedures, since no 3D reconstruction from X-ray images is required in order to perform 3D coronary motion tracking as in [7,8] and no manual segmentation or user-iteraction is required for patient-specific coronary motion modeling. Secondly, by combining greylevel CTA image, its vesselness response image and coronary probability atlas in the proposed registration framework, this approach provides a robust estimation of the coronary motion in 4D CTA.

2 Method

In order to augment the intraoperative images acquired with stereo-endoscope during TECAB procedure, a patient-specific 4D motion model of coronaries is constructed from the pre-operative dynamic CTA sequence. This is achieved by forming coronary probability atlas and using multi-channel LDDMM registration [10,11]. The formalism of LDDMM makes large diffeomorphic (smooth and invertible) transformations possible when registering two shapes. Contrary to alternative methods [12,13], the LDDMM formalism is designed to compute shape deformations that are geodesics. An optimal flow of deformation is then estimated between the source and the target images according to a regularization metric and a similarity measure. Being able to follow the coronary motion using this formalism then offers new possibilities for the statistical characterization of this motion. However, in this context and for coronary motion tracking from CTA sequences, mono-channel registration on the grey level images does not capture accurately the highly localized coronary motion which is surrounded by large anatomical structures . The method in [10] has previously been extended to treat multi-channel images [11]. Our methodological contribution is then to use multi-channel registration, where each channel contains a level of description of the registered shapes: (1) original images, (2) coarse but robust extractions of the coronary vessels and (3) highly smoothed original images. We then denote our approach as Multi Level- or ML-LDDMM.

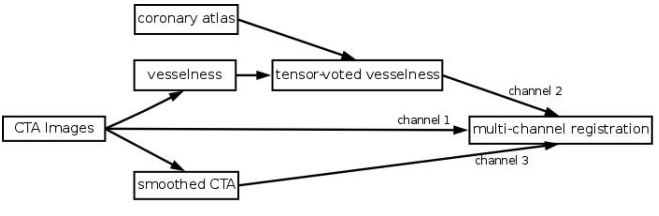

Fig. 1. Overview of the proposed coronary motion estimation method

By using tensor voting and extracting the largest connected components, the coronary lumen is segmented from the post-processed vesselness response image at end-systolic phase for each 4D CTA sequence. The segmented coronary lumen is then transformed to the end-diastolic time frame according to the deformation from ML-LDDMM registration. The estimated coronary lumen at end-diastolic is then compared to manual tracking of the coronaries at end-diastolic phase. Fig. 1 shows an overview and illustrates the connections between the components in our proposed algorithm.

2.1 Coronary Atlas Construction Using Affine Registration

Chillet *et al* [14] presented a method for forming brain and liver vascular atlases using a vessel-to-image affine registration method. Here a 3D probability atlas $\mathcal{A}$ containing left anterior descending (LAD), left circumflex artery (LCX) and right coronary artery (RCA) is constructed from the manually marked centerlines in a group of single-phased 3D CTA scans acquired from 26 patients. One subject's CTA scan is chosen as reference $\mathcal{R}$ and the rest of the CTA scans are affine aligned with $\mathcal{R}$. The manually segmented centerlines are transformed according to the resulting affine transformation in order to match with the centerline from the reference subject. All the transformed centerlines and the corresponding reference centerline are then wrapped as a tubular structure with a pre-defined radius and blurred with Gaussian kernel. For each coronary artery, the blurred tubular structures are averaged together using a Gaussian kernel to create the atlas for that branch. The process is repeated for all three coronary arteries, LAD, LCX and RCA in order to form a probability atlas for coronary tree.

By affine alignment of the reference image $\mathcal{R}$ used for creating the probability atlas and the end-diastolic phase of a new patient CTA sequence, this atlas $\mathcal{A}$ is affinely registered to the patient dataset to create patient-specific coronary mask $\mathcal{M}_{ED}$. For each patient CTA sequence, the 3D mask $\mathcal{M}_{ED}$ is then warped to create a mask $\mathcal{M}_{SD}$ corresponding to end-systolic phase by non-rigid registration [15] of the CTA images. Each patient-specific coronary mask is then used to select the coronary artery region from its corresponding vessel response image and incorporated in the ML-LDDMM registration.

2.2 Multi-scale Vessel Enhancement Diffusion and Filtering

Prior to the coronary artery segmentation, vessel enhancing diffusion [16] is used to improve the visibility of the coronaries in CTA images. To reduce the effect of the presence of inhomogeneous background (e.g. air and tissue mixed region) or irrelevant neighboring structures (e.g. bone or metal implant), multiple thresholds are selected automatically by 4D multi-level thresholding extended from Otsu's method [17] for each 4D data set. The intensities of the background voxels are increased so that they match the average myocardial intensity level. Voxels with intensities above the upper threshold level that represents bone structure are assigned average myocardium intensity value.

We perform a coarse segmentation of the coronary arteries in the CTA image using a multiscale Hessian-based vessel enhancement filter [18]. The filter

utilizes the 2nd-order derivatives of the image intensity after smoothing (using a Gaussian kernel) at multiple scales to identify bright tubular-like structures with various diameters. The six second-order derivatives of the Hessian matrix at each voxel are computed by convolving the image with second-order Gaussian derivatives at pre-selected scales. Assuming a 3D image function $I(x)$, the Hessian matrix at a given voxel x at scale σ is denoted as $H_\sigma(x)$. A vesselness term $V(x)$ is defined as in Frangi *et al.* [18] and is based on the eigenvalues and eigenvectors of $H_\sigma(x)$. The vesselness response is computed at a range of scales, exponentially distributed between σ_{min} and σ_{max} . The maximum response with the corresponding optimal scale is obtained for each voxel of the image. The vesselness image is then constructed using the maximum response of each voxel as the intensity value.

2.3 Tensor Voting

Due to artifacts introduced in CT reconstruction and the low signal-to-noise ratio in certain phases caused by the application of ECG pulsing windows to reduce the radiation dose for the patient [19], segmenting the vessels directly from the vesselness images does not provide satisfactory results. To alleviate those effects, we propose to use a post-processing step of tensor voting [20,21] to enhance the extraction of the coronary vessels. Tensor voting was initially developed to reconstruct shapes from point clouds but was also shown efficient to recover volumes, surfaces and curves from noisy images. Here it is adapted to fill discontinuities in vesselness response image.

Consider a vesselness image $I_v \in \Omega$. We associate a tensor-valued image $\boldsymbol{TV} \in \Omega$ to I_v. Each voxel of $\boldsymbol{TV}$ is a 3×3 matrix that allows the local communication between the noisy data of I_v. Using the framework of [21], each non-null voxel x_i of I_v is considered as an island token i, where $i \in \{1, ..., N\}$. A token is then here a point being potentially in a curve according to the vesselness image. This token generates a tensor field $\boldsymbol{TV}_i$ around x_i. For $x \in \Omega$, $\boldsymbol{TV}_i(x)$ is computed as the tensor product of a vector $\boldsymbol{W}_i(x)$ with itself. This vector is defined as:

$$\boldsymbol{W}_i(x) = e^{-\frac{d(x_i,x)^2}{\delta^2}} \frac{x_i x}{d(x_i, x)}, \tag{1}$$

where $d(x_i, x)$ is the Euclidian distance between x_i and x and δ is a scale at which the structures are recovered. In our computations, we set δ to values slighly higher than the typical radius of the vessels. Note that in practice, we only compute $\boldsymbol{TV}_i(x)$ in a bounding box in which its values are not negligible. The communication between the island tokens is then performed in $\boldsymbol{TV}$ by using:

$$\boldsymbol{TV}(x) = \sum_{i=1}^{N} \boldsymbol{TV}_i(x), \quad \forall x \in \Omega. \tag{2}$$

By using the saliency map to a curve: $L(x) = \lambda_1(x) - \lambda_2(x)$, where $\lambda_1(x)$ and $\lambda_2(x)$ are the two highest eigenvalues of $\boldsymbol{TV}(x)$, we finally measure how the point x fits into a curve according to its neighborhood. This map enhances the

coronary vessels even where the contrast between the vessels and the surrounding tissues is low. Note that this simple interpretation of the tensor voting generates a small ghosting effect around the vessel centerlines. So $L(x)$ is smoothed with a Gaussian filter of standard deviation $\delta/2$.

2.4 Multi level LDDMM Registration

Image registration is performed using three channels ($C_{1,S}$, $C_{2,S}$, $C_{3,S}$) and ($C_{1,T}$, $C_{2,T}$, $C_{3,T}$) computed from the source image I_S and the target image I_T using the pipeline summarized in Fig. 1 and explained in the previous subsections. The first channel C_1 contains the original images I_S and I_T. The second one contains the enhanced vesselness images L_S and L_T, calculated in subesction 2.3. Finally, the third channel represents the original images smoothed by a large gaussian filter (5mm in our calculations). These channels are a multi-level representation of the registered shapes. The channel C_3 pushes the source image to the target image without any consideration of the details, so the global motion of the large components of the CTA images is tracked. The channel C_2 has a similar role, but only focuses on the coronary region. Finally, the channel C_1 is complementary to C_2 and C_3 since it takes image details into account.

A multi-level strategy, as in Fig. 2, is adopted to register the images efficiently. In the first level, an initial estimation of optimal deformation is obtained using the smoothed images C_3, then this estimation is refined using registration based on the second channel C_2. Finally by introducing channel C_1, all the information is taken into account for the finest estimation of deformation. This strategy is particularly robust. For the first two levels, it can be performed on down-sampled images speedily without losing much accuracy.

The registrations are performed using the LDDMM framework [10,11]. In this framework, the images are deformed through time dependent diffeomorphic transformations ϕ_t, $t \in [0, 1]$, which are defined by a time dependent velocity field

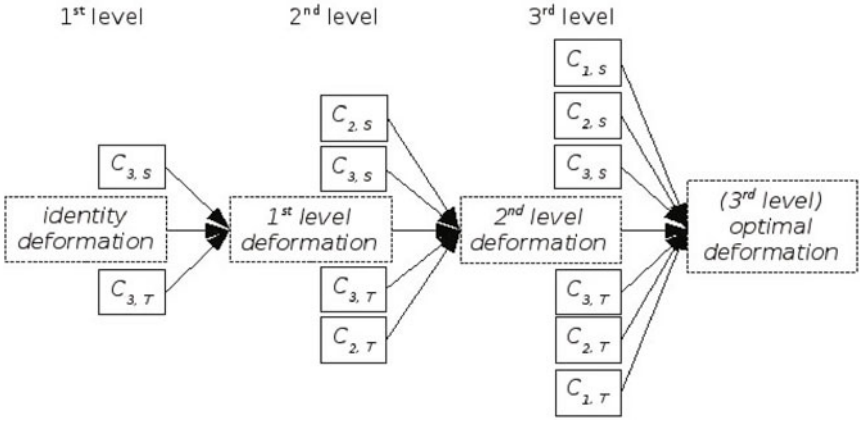

Fig. 2. Multi-level strategy of the registration

v as follows: $\partial_t \phi_t = v_t(\phi_t)$, where ϕ_0 is the identity deformation and $t \in [0,1]$. The velocity field v_t deforms the image coordinates at time t and ϕ_t is the induced deformation. For notational convenience, we introduce $\phi_{t,s} \doteq \phi_s \circ \phi_t^{-1}$. Contrary to [10], where the similarity measure is computed directly from I_S and I_T, the images are indirectly compared here using the information contained in the channels. The energy we minimize, as a function of v, is then:

$$E(v) = \int_0^1 \frac{1}{2}||v_t||_V^2 \mathrm{d}t + \sum_{i=1}^{3} \left(\alpha_i ||C_{i,S} \circ \phi_1^{-1} - C_{i,T}||_{L^2}^2\right), \tag{3}$$

where $\alpha_i \in [0,1]$, controls the weight of the channel i. These weights are tuned to have a similar influence of each channel. In the energy of the deformations, the time dependent velocity field v is assumed to lie in $L^2([0,1],V)$, where V is a Hilbert space of vector fields. Underlying this space, there exists a smooth matrix valued kernel K that controls the spatial correlation of the deformations. The minimization of the energy is described hereafter.

We denote $D_t^{i,S} = C_{i,S} \circ \phi_{t,0}$ and $D_t^{i,T} = C_{i,T} \circ \phi_{1,t}$. The Jacobian of $\phi_{t,1}$ at time t is also noted $|D\phi_{t,1}|$. The minimization of the variational problem of Eq. 3 is performed by using a steepest gradient descent approach. Practical resolution then involves the iterative use of the gradient of the functional E at time t:

$$\nabla_v E_t = v_t - K \star \left(|D\phi_{t,1}| \sum_{i=1}^{3} (\alpha_i \nabla D_t^{i,S} (D_t^{i,S} - D_t^{i,T})) \right), \tag{4}$$

where $\star$ is the convolution operator. In our computations, we used an isotropic Gaussian kernel K of standard deviation 10mm. Such kernel offers a good balance between enough spatial correlation to ensure vessel radius preservation and enough spatial flexibility to properly match curved vessels.

3 Results and Evaluation

The coronary atlas is constructed from the CTA scans of 26 patients. The proposed motion estimation algorithm is tested in 4D CTA sequences from eight subjects. For each subject, we segmented the coronary lumen automatically and performed a thinning algorithm to get the coronary tree centerlines from both

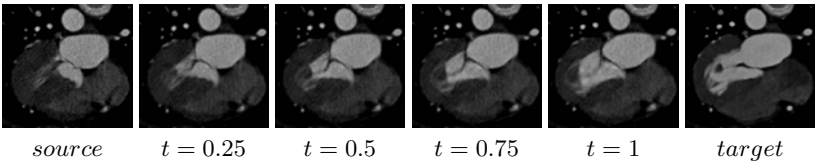

Fig. 3. ML-LDDMM registration results. From left to right, source image I_S, intermediate transformed results ($t = 0.25, 0.5, 0.75$), final result ($t = 1$) and target image I_T

end-systolic (ES) and end-diastolic (ED) phases. The centerlines in ES phase are then deformed according to the optimal deformation from ML-LDDMM registration to estimate the coronary positions in ED phase.

In order to quantitatively measure the accuracy of the motion tracking algorithm, we manually marked the centerlines for the ED and ES phases in these eight CTA sequences. We compare the transformed centerlines with the manually marked ones in ED phase as in the third row of Table 1. The distance between the manual segmentation U and the automatic tracked coronaries W in each time frame is measured as:

$$D(W, U) = \frac{1}{N_W} \sum_{i=1}^{N_W} \|w_i - l(w_i, U)\|_2 + \frac{1}{N_U} \sum_{j=1}^{N_U} \|u_j - l(u_j, W))\|_2 \quad (5)$$

where N_W and N_U are the number of points representing vessel W and vessel U correspondingly. For each point $m_i \in W$, $l(m_i, U)$ calculates the closest point to w_i on the automatically extracted vessel U. Similarly, for each point $u_j \in U$, $l(u_j, W)$ defines the closest point to u_j on the vessel W. As comparison, we

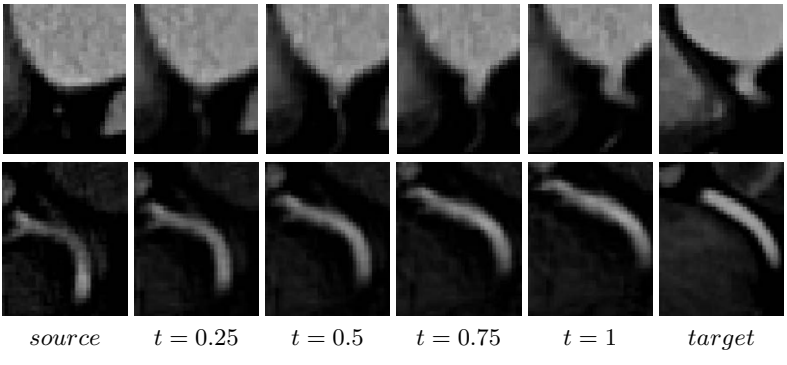

Fig. 4. Registration results. The top row shows starting position of RCA. From left to right, the source image, the intermediate transformed source images ($t = 0.25, 0.5, 0.75$), the final result ($t = 1$) and the target image. Similarly, the bottom row shows the mid-section region of RCA deforming from source to match with target. Note that in each row all images were taken in the same region of interest.

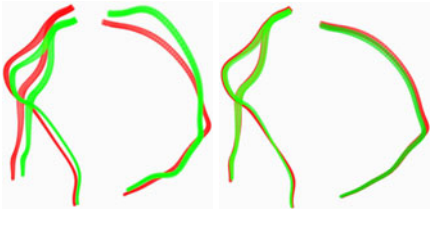

Fig. 5. Coronary artery lumen (P6). Left: segmented coronary artery lumen at ES (green) and ED (red) phases. Right: estimated coronary lumen at ED phase (green) compared with segmented lumen at ED (red).

Table 1. Coronary displacement and error of motion estimation

	P1	P2	P3	P4	P5	P6	P7	P8
Displacement (mm)	8.18	7.63	8.36	7.79	8.62	10.05	8.09	7.88
Estimation error (mm)	1.79	1.26	1.43	1.25	0.69	1.19	1.35	1.04
Compensation (%)	78.12	83.49	82.89	83.95	92.00	88.16	83.31	86.80

also present the natural displacement of coronary tree from ES to ED as in the second row in Table 1. The fourth row shows the percentage of coronary displacement that has been compensated by our motion estimation method. The results show that ML-LDDMM registration based motion estimation has performed robustly and accurately. By automatically segmenting the coronary artery and tracking the coronaries from ES to ED in CTA sequences, the patient-specific coronary model and motion estimation are performed robustly in all eight testing subjects.

4 Discussion

We have presented a novel approach for patient-specific coronary artery segmentation and motion estimation from dynamic cardiac CTA sequences that significantly improves the robustness of motion tracking and eliminates the manual interaction. The proposed method has been tested on the clinical CTA datasets acquired from eight subjects. By segmenting coronaries and tracking their motion from pre-operative cardiac images and aligning this motion with the series of 2D endoscopic images capture during the operation, we aim to assist the surgical planning and provide image guidance in robotic-assisted totally endoscopic coronary artery bypass (TECAB) surgery. Through this work, we expect to reduce the conversion rate from TECAB to conventional invasive procedures.

References

1. Mohr, F.W., Falk, V., Diegeler, A., Walther, T., Gummert, J.F., Bucerius, J., Jacobs, S., Autschbach, R.: Computer-enhanced "robotic" cardiac surgery: Experience in 148 patients. J. Thorac. Cardiovasc. Surg. 121(5), 842–853 (2001)
2. Dogan, S., Aybek, T., Andressen, E., Byhahn, C., Mierdl, S., Westphal, K., Matheis, G., Moritz, A., Wimmer-Greinecker, G.: Totally endoscopic coronary artery bypass grafting on cardiopulmonary bypass with robotically enhanced telemanipulation: Report of forty-five cases. J. Thorac. Cardiovasc. Surg. 123, 1125–1131 (2002)
3. Feyter, P.J., Krestin, G.P. (eds.): Computed Tomography of the Coronary Arteries, 2nd edn. Informa Healthcare (2008)
4. Schaap, M., Metz, C., van Walsum, T., van der Giessen, A., Weustink, A., Mollet, N., Bauer, C., Bogunovifa, H., Castro, C., Deng, X., Dikici, E., ODonnell, T., Frenay, M., Friman, O., Hernandez Hoyos, M., Kitslaar, P., Krissian, K., Kuhnel, C., Luengo-Oroz, M., Orkisz, M., Smedby, O., Styner, M., Szymczak, A., Tek, H., Wang, C., Warfield, S., Zambal, S., Zhang, Y., Krestin, G., Niessen, W.: Standardized evaluation methodology and reference database for evaluating coronary artery centerline extraction algorithms. Med. Image Anal. 13(5), 701–714 (2009)

5. Lesage, D., Angelini, E.D., Funka-Lea, G., Bloch, I.: A review of 3D vessel lumen segmentation techniques: Models, features and extraction schemes. Med. Image Anal. 13, 819–845 (2009)
6. Metz, C., Schaap, M., van Walsum, T., van der Giessen, A., Weustink, A., Mollet, N., Krestin, G.P., Niessen, W.: Editorial: 3D segmentation in the clinic: A grand challenge II - coronary artery tracking. In: MICCAI 2008 Workshop Proceedings (2008)
7. Shechter, G., Devernay, F., Quyyumi, A., Coste-Maniere, E., McVeigh, E.: Three-dimensional motion tracking of coronary arteries in biplane cineangiograms. IEEE Trans. Med. Imaging 22(4), 493–603 (2003)
8. Shechter, G., Resar, J.R., McVeigh, E.R.: Displacement and velocity of the coronary arteries: cardiac and respiratory motion. IEEE Trans. Med. Imaging 25, 369–375 (2006)
9. Metz, C., Schaap, M., Klein, S., Neefjes, L., Capuano, E., Schultz, C., van Geuns, R.J., Serruys, P.W., van Walsum, T., Niessen, W.J.: Patient specific 4D coronary models from ECG-gated CTA data for intra-operative dynamic alignment of CTA with X-ray images. In: Yang, G.-Z., Hawkes, D., Rueckert, D., Noble, A., Taylor, C. (eds.) MICCAI 2009. LNCS, vol. 5761, pp. 369–376. Springer, Heidelberg (2009)
10. Beg, F.M., Miller, M.I., Trouvé, A., Younes, L.: Computing large deformation metric mappings via geodesic ows of diffeomorphisms. International Journal of Computer Vision 61(2), 139–157 (2005)
11. Ceritoglu, C., Oishi, K., Li, X., Chou, M., Younes, L., Albert, M., Lyketsos, C., van Zijl, P., Miller, M., Mori, S.: Multi-contrast large deformation diffeomorphic metric mapping for diffusion tensor imaging. Neuroimage 47(2), 618–627 (2009)
12. Avants, B.B., Epstein, C.L., Grossman, M., Gee, J.C.: Symmetric diffeomorphic image registration with cross-correlation: Evaluating automated labeling of elderly and neurodegenerative brain. Med. Image Anal. 12, 26–41 (2008)
13. Vercauteren, T., Pennec, X., Perchant, A., Ayache, N.: Diffeomorphic demons: Efficient non-parametric image registration. NeuroImage 45(1), S61–S72 (2009)
14. Chillet, D., Jomier, J., Cool, D., Aylward, S.R.: Vascular atlas formation using a vessel-to-image affine registration method. In: Ellis, R.E., Peters, T.M. (eds.) MICCAI 2003. LNCS, vol. 2878, pp. 335–342. Springer, Heidelberg (2003)
15. Rueckert, D., Sonoda, L.I., Hayes, C., Hill, D.L., Leach, M.O., Hawkes, D.J.: Non-rigid registration using free-form deformations: application to breast MR images. IEEE Trans. Med. Imaging 18(8), 712–721 (1999)
16. Manniesing, R., Viergever, M., Niessen, W.: Vessel enhancing diffusion - a scale space representation of vessel structures. Med. Image Anal. 10, 815–825 (2006)
17. Otsu, N.: A threshold selection method from gray-level histograms. IEEE Transactions on Systems, Man and Cybernetics 9(1), 62–66 (1979)
18. Frangi, A., Niessen, W., Hoogeveen, R., van Walsum, T., Viergever, M.: Model-based quantitation of 3D magnetic resonance angiographic images. IEEE Trans. Med. Imaging 18(10), 946–956 (1999)
19. Weustink, A.C., Mollet, N.R., Pugliese, F., Meijboom, W.B., Nieman, K., Heijenbrok-Kal, M.H., Flohr, T.G., Neefjes, L.A., Cademartiri, F., de Feyter, P.J., Krestin, G.P.: Optimal electrocardiographic pulsing windows and heart rate: Effect on image quality and radiation exposure at dual-source coronary CT angiography. Radiology 248(3), 792–798 (2008)
20. Jia, J., Tang, C.: Image repairing: Robust image synthesis by adaptative ND tensor voting. In: IEEE CVPR, vol. 1, p. 643 (2003)
21. Risser, L., Plouraboue, F., Descombes, X.: Gap filling of 3-D microvascular networks by tensor voting. IEEE Trans. Med. Imaging 27(5), 674–687 (2008)